Science and Technology Indonesia
e-ISSN:2580-4391 *p*-ISSN:2580-4405
Vol. 10, No. 4, October 2025

Research Paper

Development of Nanofiber Made of Nanocellulose with Oil Encapsulation of *Eucalyptus* sp.

Wida Fatma Sari[1,2], Sri Haryati[3*], Risfidian Mohadi[4]

[1]*Student Doctor of Chemical Engineering, Graduate Program, Universitas Sriwijaya, Palembang, 30139, Indonesia*
[2]*Department of Chemical Engineering, Universitas PGRI, Palembang, 30136, Indonesia*
[3]*Department of Chemical Engineering, Universitas Sriwijaya, Palembang, 30139, Indonesia*
[4]*Master of Materials Science, Graduate Program, Universitas Sriwijaya, Palembang, 30139, Indonesia*
***Corresponding author**: haryati_djoni@yahoo.co.id

Abstract
The amalgamation of natural polymers derived from lignocellulosic waste with synthetic polymers is a potential avenue for producing high-value products through nanotechnological innovations. Nanofibers are a significant application of nanotechnology and is now being explored as an alternative method for treating lignocellulosic waste. Nanofiber is a fiber generated by an electrospinning device. Cellulose obtained from lignocellulose can be transformed into valuable products, including nanocellulose. This project entails the synthesis of nanofibers via the combination of natural and synthetic polymers, an innovative approach in the field. Natural polymers are derived from alginate and nanocellulose, whilst synthetic polymers are produced from Poly Vinyl Alcohol (PVA). This study employs nanofibrils in healthcare, specifically as a cartridge filter in masks infused with *Eucalyptus* sp. This study sought to identify the optimal method for producing nanofibers with a minimal pore size by varying the concentrations of PVA (4%, 8%, 12%, and 16%) and nanocellulose (2.5%, 5%, and 7.5%). This research employs a combination of methods to produce nanocellulose of suitable size, an innovative process. The pretreatment process utilizes a blend of chemical and physical methods. Nanocellulose is synthesized using varying concentrations of sulfuric acid (25%, 50%, and 75%) during the acid hydrolysis process. The optimal nanocellulose size was attained at a sulfuric acid concentration of 50% (40°C, 10 minutes), as evidenced by a mean diameter of 484.3 nm. The amalgamation of physical and chemical methods has demonstrated efficacy in generating a beneficial pore size distribution in nanocellulose. Nanofibers are synthesized utilizing 12% PVA, 0.5% alginate, 2.5% nanocellulose, and 1% *Eucalyptus* sp. over 30 hours (3 mL), resulting in an average diameter of 200 nm for the created nanofibers. Concurrently, the nanofiber produced in the absence of *Eucalyptus* sp. exhibited a diameter of 240 nanometers.

Keywords
Nanofiber, Nanocellulose, Electrospinning, Encapsulation, Tissue Engineering

Received: 12 November 2024, Accepted: 2 July 2025
https://doi.org/10.26554/sti.2025.10.4.1074-1086

1. INTRODUCTION

Palm oil is a highly coveted commodity among investors owing to its substantial worth (Syahza and Asmit, 2020). The palm oil industry in Indonesia requires focused scrutiny due to its environmental consequences, particularly concerning Oil Palm Empty Fruit Bunches (OPEFB) and their substantial waste (Meijaard et al., 2020). The growing interest in nanofiber production predominantly employs various natural and synthetic polymers for tissue engineering (Kazemzadeh et al., 2022). Cellulose is a naturally occurring polymer used. In recent years, there has been an increasing focus on the valorization of this agricultural waste (Blasi et al., 2023). Among the promising avenues is the extraction of cellulose from OPEFB, which can serve as a valuable raw material for advanced materials such as nanofibers. The increasing interest in nanofiber production primarily utilizes various natural and synthetic polymers for applications in tissue engineering. Cellulose, a naturally occurring and biodegradable polymer, has attracted significant attention due to its abundance, renewability, and exceptional mechanical properties (Tu et al., 2021).

Nanotechnology encompasses various forms, including nanoparticles, nanofibers, nanowires, and nanotubes (Shoukat and Khan, 2021). Nanofiber is a nanomaterial that remains the subject of significant research and development efforts. Nanofibers are utilized across multiple sectors, including textiles (Mallakpour et al., 2021), composites, automotive (Natrayan et al., 2021) paper, electronics, optics, agriculture, cosmetics, health-

care, medicine, sports, and pharmaceuticals (Tuhmaz, 2024). Nanofibers can be generated using an electrospinning device (Patel et al., 2021). Electrospinning is an effective technique for enhancing the performance of cellulose nanofiber sheets, offering a viable alternative approach (Wang et al., 2021).

Nanocellulose functions as a reinforcing agent in bionanomaterials. This arises from the advantages of its mechanical properties, biocompatibility, surface chemistry, and advantageous optical characteristics (Aisy et al., 2024). Research on nanocellulose has successfully employed acid hydrolysis methods (Pawcenis et al., 2022), producing microcrystalline cellulose with dimensions ranging from 150 to 200 nm using sulfuric acid. Low et al. (2022) established that prolonging the duration of ultrasonication led to a decrease in the size of the Nanocellulose generated.

Numerous outbreaks of upper respiratory tract infections encompass the SARS-CoV-2 virus (often known as "Covid-19"), the avian influenza virus (H7N9), and the Middle East respiratory sickness (MERS) coronavirus (Flerlage et al., 2021). The mask's filtration can be improved by employing a filter cartridge to capture virus-sized particles that affect the upper respiratory tract efficiently (Goscianska et al., 2022). Cartridge filters may be used therapeutically with the inclusion of *Eucalyptus* sp. This innovation utilizes the significant cellulose content in Oil Palm Empty Fruit Bunches (OPEFB) waste, which is converted into nanocellulose fibers (filter cartridges) integrated into the mask's core to improve efficacy in filtering viruses and antiviral treatments aimed at the upper respiratory tract.

Filter cartridge sheets are infused with essential oil *Eucalyptus* sp. demonstrating antibacterial efficacy against pathogenic microorganisms (Liñán-Atero et al., 2024) in the upper respiratory tract, reducing exposure to the virus. *Eucalyptus* sp. is a genus of flora within the Myrtaceae family (Delgado-Paredes et al., 2021). *Eucalyptus* sp. is commonly employed as a medicinal herb. *Eucalyptus globulus* is a species used as a medicinal agent (Jafari et al., 2021).

The essential oil primarily consisted of oxygenated monoterpenes, monoterpenes, and oxygenated sesquiterpenes. Among these chemicals, 1.8-Cineol (72.71%), α-terpineol (2.54%), terpinene-4-ol (0.34%), and linalol (0.24%) were identified as the predominant constituents (Park et al., 2024). The predominant oxygenated monoterpenes identified were α-eudesmol (0.39%), globulol (2.77%), and epilobulol (0.44%), which were the leading sesquiterpenes. The identified significant compounds are: α-terpineol acetate (3.1%), geranyl acetate (0.71%), L-pinocarveol (0.36%), β-sabinene (0.25%), and terpinolene (0.19%). Nevertheless, a portion (0.26%) of the total components remains unidentified (Malakar, 2024). Chemical constituents in the Fruit of *Eucalyptus* sp. Fifteen compounds were obtained and identified as outlined below: beta-sitosterol, betulinic acid, stigmasterol, euscaphic acid, 2α-hydroxybetulinic acid, macrocarpol B, macrocarpal A, oleanolic acid, 3.4.3-O-trimethylellagic acid, 3-O-methylellagic acid 4-O-(2-O-acetyl) –alpha-L rhamnopyranoside, 3-O-methylellagic acid, ellagic acid, and gallic acid (Veerendranadh et al., 2018).

The essential oil extracted from the leaves of *Eucalyptus* sp. is employed in the treatment of pulmonary tuberculosis (Dheyab et al., 2022), diabetes (Kim et al., 2020), influenza (Galan et al., 2020), antiseptic applications (Pimenta et al., 2023), asthma (Galan et al., 2020), and as a disinfectant (Aminsobhani et al., 2022). It is also used in malaria therapy (Deligianni et al., 2023), and possesses antibacterial, antifeedant, antifungal (Rawat et al., 2022), and repellent (Rehman et al., 2024) properties. The stem is utilized for its antiviral effects (Maftuchah et al., 2020).

This study aims to synthesize nanocellulose fiber sheets from OPEFB via the electrospinning technique to create fiber sheets capable of encapsulating *Eucalyptus* sp. The sheet is intended for therapeutic use in the upper respiratory system. This study involves the manufacture of nanofibril nanocomposites by integrating a PVA polymer matrix with nanocellulose and alginate, resulting in nanofibril cellulose sheets characterized by optimal pore topologies. This study involves the manufacture of nanocellulose fibers from OPEFB by synergizing chemical and physical methods to achieve. Nanocellulose with improved particle size, crystalline, efficacy, and purity. This work is distinctive as it integrates a PVA polymer matrix with natural polymers, specifically nanocellulose and alginate while varying the amounts of each polymer.

This investigation was conducted by integrating chemical and physical approaches. The chemical approach employs acidic and basic solutions. The treatment of OPEB involves dissolution in a 2.5% sodium hypochlorite (b/v) solution. The mixture is subsequently refluxed with 17.5% sodium hydroxide. After the pretreatment step, acid hydrolysis, accompanied by ultrasonication, was selected. Nanocellulose has been combined with 100% pure *Eucalyptus* sp. merk Garden.

2. EXPERIMENTAL SECTION

2.1 Materials

Oil Palm Empty Fruit Bunches (OPEFB), Aquadest, 3.5% HNO_3, $NaNO_2$, 2% NaOH, 2% $NaSO_3$, 1.75% NaOCl, 17.5% NaOH, 10% H_2O_2 Aquabidest, 45%, H_2SO_4. *Eucalyptus globulus* Garden 100 % pure essential oil 30 mL.

2.2 Tools

Laboratory glassware, an analytical balance, standard filter paper, a thermometer, a hot plate, a pH meter, a desiccator, a centrifuge, and a sieve are among the instruments employed. The utilized instrumentation comprises a nanofibril cellulose sheet printing apparatus or electrospinning device CAAI 2601 Nachriebe 601 at the Faculty of Mathematics and Natural Sciences, University of Sriwijaya Electrospinning, Center of Aerosol and Analytical Instrumentation (CAAI), Bandung, Indonesia, a high voltage power supply, and Scanning Electron Microscopy (SEM) Bruker's electron microscope analyzers located at the South Sumatra Regional Police Forensic. Instrument Particle Size Analyzers (PSA) located at ILRC Building, University of Indonesia Campus, West Java, 16424, Indonesia.

2.3 Method

2.3.1 Nanocellulose Manufacturing Method

This research was made by combining chemical and physical methods. The chemical method uses acid and alkaline solutions. Oil Palm Empty Bunches pretreatment is dissolved with 2.5% Sodium Hypochlorite (b/v). Then, it is refluxed with 17.5% NaOH. The method chosen after the pretreatment process is acid hydrolysis and, followed by ultrasonication. Nanocellulose that has been added to *Eucalyptus globulus* Garden 100% pure essential oil 30 mL.

2.3.2 Nanofiber Manufacturing Method

In the production of nanofibers, a specific quantity of PVA and deionized water is stirred on a heated plate at 500 rpm and 80°C for 1 hour, totalling 3 mL. Subsequently, nanocellulose is incorporated and agitated at ambient temperature for one hour to produce the PVA/NC/Alginate/*Eucalyptus* sp. solution, with PVA concentrations of (4, 8, 12.16) %b/v, nanocellulose at (2.5, 5, 7.5) %b/v, alginate at 0.5 %b/v, and *Eucalyptus* sp. at 1%. The PVA/Nanocellulose/alginate/*Eucalyptus* sp. solution is degassed, put into a 20 mL syringe, and rotated within an electrospinning unit. The spinning parameters were voltage 15.1 kV, 138 counts for the high-voltage encoder, chamber temperature 26.3°C, and relative humidity 64.0% (Gupta et al., 2021).

3. RESULTS AND DISCUSSION

3.1 Nanocellulose Manufacturing

The outcomes of the acid hydrolysis procedure, which entailed protonating the acetal oxygen within the glycosidic bond, were as follows: The formation of carbocation on the anomeric carbon through heterolysis results in the breaking of glycosidic bonds. Subsequently, the carboxylation process occurs, producing a hydroxyl group and a proton.

3.2 Characterization of PSA (Particle Size Analyzer)

3.2.1 Nanocellulose

The outcomes of the acid hydrolysis process, which entailed the protonation of the acetal oxygen within the glycosidic bond, are delineated below: The nanocellulose is subsequently diluted with distilled water was added into the cuvette. Measurements are conducted at room temperature, with a range spanning from 10 nm to 4000 nm. The dimensions of nanocellulose are determined as follows.

Table 1. Results of PSA Analysis of Nanocellulose Size

Variation in H_2SO_4 Concentration	Nanocellulose Size
H_2SO_4 25%	664.8 nm
H_2SO_4 50%	484.3 nm
H_2SO_4 75%	865.5 nm

The Table 1 presents the results of nanocellulose particle size analysis obtained using a Particle Size Analyzer (PSA) across different concentrations of sulfuric acid (H_2SO_4) employed during the hydrolysis process. In this study, sulfuric acid concentrations of 25%, 50%, and 75% were applied at 40°C for 10 minutes. The concentration of sulfuric acid is a critical parameter in the acid hydrolysis of cellulose, as it directly influences the extent of fiber depolymerization and the final particle size distribution of the resulting nanocellulose. The data demonstrate a clear correlation between acid concentration and particle size. At 25% H_2SO_4, the average particle size was measured at 664.8 nm. The smallest particle size, 484.3 nm, was observed at 50% concentration, suggesting that this condition offers an optimal balance between effective hydrolysis and particle stability, facilitating the production of finer nanocellulose structures. However, at 75% H_2SO_4, the particle size increased significantly to 865.5 nm. This may be attributed to excessive acid concentration potentially inducing nanocellulose particle agglomeration, structural degradation, or partial recrystallization, possibly due to intensified hydrogen bonding between fragmented fibrils. Such effects could lead to the formation of larger or less uniform particles.

A graphical representation of the PSA results corresponding to the 25%, 50%, and 75% H_2SO_4 treatments further illustrates the influence of acid concentration on nanocellulose size distribution.

This research in Figure 1 employs an innovative process that uses a combination of methods to produce nanocellulose of a suitable size. The pretreatment process uses a combination of chemical and physical methods. Nanocellulose is synthesized by using different concentrations of sulfuric acid (25%, 50%, and 75%) during acid hydrolysis. The results of the analysis were used to produce PSA cellulose nanofibers. Based on the results of the analysis, PSA cellulose nanofibers were produced at concentrations of 25% nanocellulose size 664.8 nm, 50% nanocellulose size 484.3 nm, and 75% nanocellulose size 865.5 nm.

3.3 FTIR Characterization of Nanocellulose

In this study, it was analyzed using FTIR. The measurement results are shown in the graph below, which describes the FTIR measurements at 3 different sulfuric acid concentrations of 25%, 50%, and 75%.

In this graph Figure 2, the −OH stretching group appears at a wavelength of 1640.23, 3736.62, 1642.37, 3729.56, 1679.72 cm^{-1}. Wavelength 3300–3400 cm^{-1} –OH stretching and 1640 cm^{-1} −OH bending characteristic of pure cellulose (Md Salim et al., 2021). Then, there is a −CH Alkyl stretching group that appears at around 2800-2900 cm^{-1} −CH stretching, 1420 cm^{-1} −CH bending, 1370 cm^{-1} −CH bending (Kumar et al., 2022). Absorption bands at around 2805.03, 2968.28, 1420.83, 2805.92 cm^{-1} are CH extended vibrational peaks, CH deformations, and glucose round ring stretches from cellulose, hemicellulose, and lignin structures (Chen et al., 2022). The C−O−C eter group appears at around 1158-1160 cm^{-1} (Fletes-Vargas et al., 2023). The –OH, –CH, C−O−C, and C=C functional groups are the main groups of cellulose (Fan

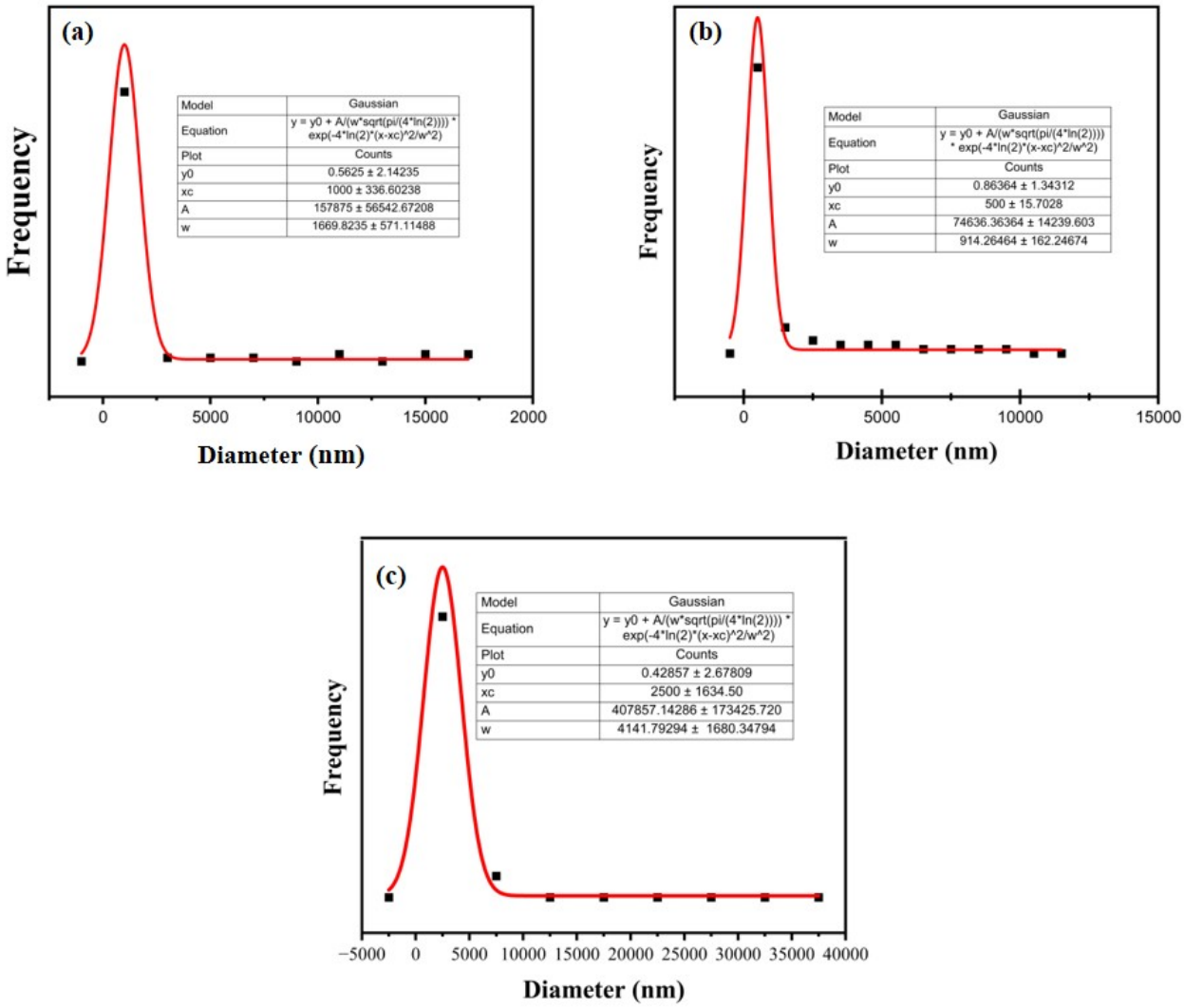

Figure 1. PSA Analysis Results in (a) Nanocellulose size 664.8 nm, (b) Nanocellulose Size 484.3 nm, (c) Nanocellulose Size 865.5 nm

et al., 2021). Figure 2 illustrates the infrared absorption spectra of nanocellulose treated with 25% sulfuric acid after OPEFB pretreatment, which involved three processes: alkaline treatment, bleaching, and hydrolysis via ultrasonication. The preliminary alkaline treatment, defined by the elimination of hydroxyl groups by a reaction with sodium hydroxide, decreases hydrogen bonds due to their dissociation. The presence of hydroxyl (OH) functional groups, indicative of alkaline treatment, is confirmed by the FTIR spectrum, exhibiting a characteristic absorption band within the range of 3736.62 cm^{-1}. In cellulose, most –OH groups are bound through hydrogen bonds between chains, resulting in a broad O–H stretching band around 3200–3500 cm^{-1}. However, a small, sharp peak at approximately 3700 cm^{-1} also appears in the FTIR spectrum (Vârban et al., 2021). This peak is attributed to free –OH surface groups on cellulose that do not participate in hydrogen bonding. For example, hydroxyl groups on the surface of cellulose fibrils, at the chain ends, or in crystalline regions where hydrogen bonds are imperfectly formed (Zhou et al., 2024). Subsequently, a bleaching process is undertaken as a secondary treatment step to further eliminate residual lignin content from the material. The cluster analysis revealed the existence of lignin in OPFEB nanocellulose. The results indicate that the bleaching technique is insufficient, as demonstrated by the presence of lignin in the final nanocellulose product, evidenced by the spectra at 1652.41cm^{-1}. The C−O−C eter group appears at around 1159.51 cm^{-1}. The lack of a –SO and C=C link in the hydrolysis of nanocellulose acid indicates that the process may be inefficient (Bacha, 2022). The spectrum of the sample displays a peak at approximately 1550.65 cm^{-1},

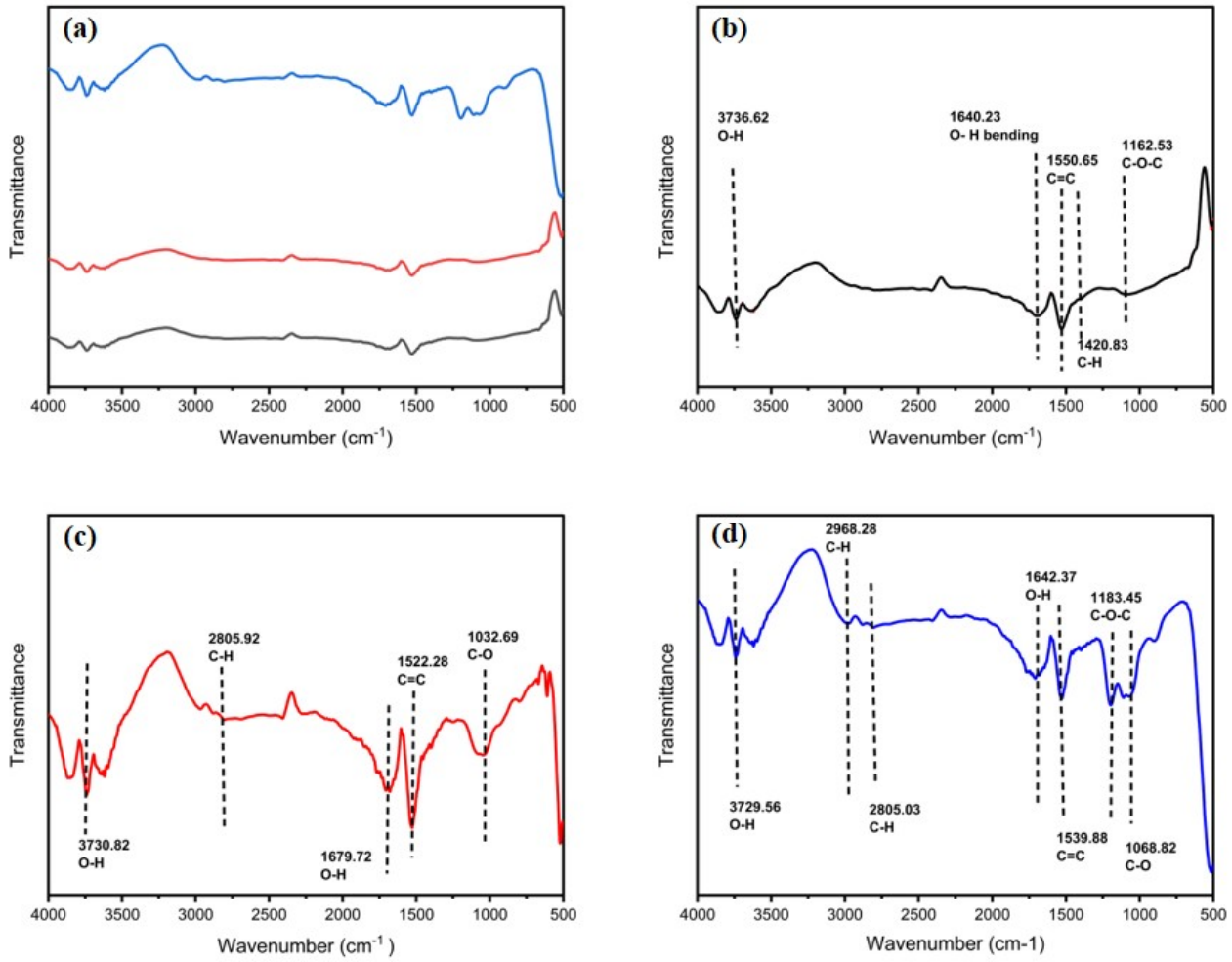

Figure 2. Nanocellulose Infrared Absorption Area with (a) Combine 3 Sample (b) 25%, (c) 50%, (d) 75% Sulfuric Acid Hydrolysis

indicative of the presence of lignin and hemicellulose, given the 25% H_2SO_4 concentration. The aromatic structure of lignin contributes to its distinctive spectrum.

The infrared absorption spectra of nanocellulose subjected to 50% sulfuric acid hydrolysis. The infrared absorption spectra of nanocellulose treated with 50% sulfuric acid indicates that the initial alkaline treatment diminishes hydrogen bonding by eliminating hydroxyl groups through a reaction with sodium hydroxide (Zhou et al., 2024). The −OH stretching group appears at a wavelength of 1679.72, 3730.82 cm^{-1}.The subsequent phase is bleaching. Bleaching seeks to eliminate lignin content. The FTIR spectrum data indicated the presence of an carbonyl C−O functional group at a wavelength of 1032.69 cm^{-1} (Pimenta et al., 1998). The cluster stated the presence of lignin in OPEFB Nanocellulose. The current bleaching method is insufficient, resulting in the final nanocellulose product retaining lignin at spectral peaks of 1522,28 cm^{-1}. The C−O−C eter group appears at around 1032.69 cm^{-1}. The hydrolysis of nanocellulose acid indicates the absence of the $-SO_3$ bond, signaling that sulfate esterification during washing is optimized. When sulfuric acid is diluted with water, it generates an H_3O^+ ion that subsequently engages with a cellulose ring to establish an O−H bond (Wohlert et al., 2022). This reaction generates H_2O, which then engages with the cellulose ring, forming an O−H bond and liberating H^+ ions (Zhang et al., 2024). Fifty percent sulfuric acid maintains the cellulose structure while effectively removing lignin and hemicellulose.

The infrared absorption spectra of nanocellulose subjected to 75% sulfuric acid hydrolysis indicates the presence of an OH group, suggestive of alkaline treatment, evidenced by absorption peaks at 1642.37, 3729.56 cm^{-1}. The secondary treatment is bleaching, which is aimed at removing the lignin component (Susi et al., 2022). The FTIR spectral data validated the existence of an alkyl C−H functional group, indicated by absorption peaks at 2848-2916 cm^{-1} (Kumar et al., 2022). The absorption bands observed at 2805.03, 2968.28 cm^{-1} are attributed to CH extended vibrational peaks, CH deformations, and glucose ring stretches from cellulose, hemicellulose,

and lignin structures, respectively (Aisy et al., 2024). Cluster analysis showed the presence of lignin in TKKS Nanocellulose. The FTIR spectral analysis indicated the existence of a C=C alkyl aromatic functional group within the wavelength 1539.88 cm^{-1}. The C−O−C eter group appears at around 1183.45 cm^{-1}. This result suggests the bleaching process is inadequate, as the resulting nanocellulose product retains lignin. Spectrum: 1539.88 cm^{-1} also the absence of a $–SO_3^-$ bond in the hydrolysis of nanocellulose acid signifies that sulfate esterification is the predominant process during the washing phase. The dilution of sulfuric acid with water produces an H_3O^+ ion, which then engages with a cellulose ring to form an O−H bond.

3.4 FTIR Characterization of Nanocellulose and *Eucalyptus*. sp

The image below is from an FTIR analysis that assessed the structural and functional groups of the nanocellulose and eucalyptus oil composite.

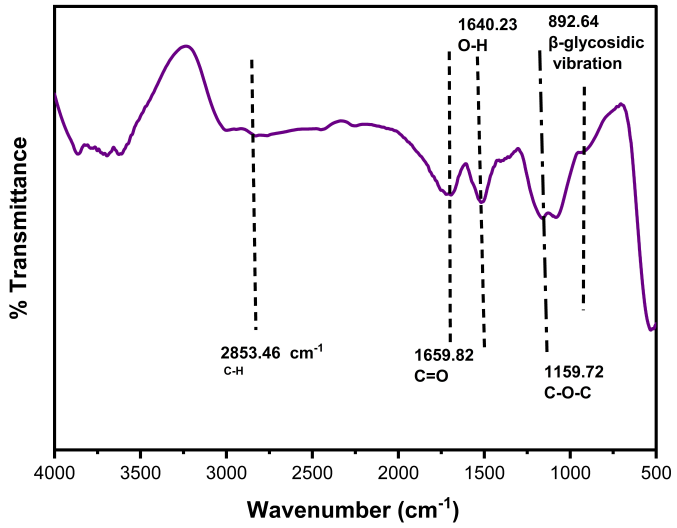

Figure 3. FTIR Characterization of Nanocellulose and *Eucalyptus* sp.

The spectral data from FTIR Figure 3 reveal the existence of the carbonyl (C=O) stretch 1659.63 cm^{-1} and the symmetrical deformation of CH_3 at peaks 2853.46 cm^{-1}. The symmetrical 1159.72 cm^{-1} stretches of C–O–C, as well as the deformations of CH alkyl deformation at 2853.46 cm^{-1} and O−H 3342.21 cm^{-1}, are observed in the nanofiber membranes produced from eucalyptus oil and Nanocellulose (Elbhnsawi et al., 2023). A mixture of Nanocellulose and eucalyptus oil was subjected to several morphological and physical characterization assessments. The FTIR spectra reveal that the peak at 3342.21 cm^{-1} for eucalyptus oil/Nanocellulose oil is associated with O–H. Vibration of the cellulose matrix under tensile stress. The peak at 2853.46 cm^{-1} corresponds to the CH stretch, the peak at 1659.82 cm^{-1} (Apiratikul et al., 2025).

3.5 Nanofibril Cellulose

3.5.1 Nanofibril Cellulose from PVA/NC/Alginate/ *Eucalyptus* sp. Encapsulation

The hydrophilic attributes of cellulose enhance the material qualities of nanofibril cellulose sheets, rendering nanocellulose an optimal selection for their fabrication. The results demonstrate that nanofibers were effectively synthesized utilizing a formulation of 12% PVA, 0.5% alginate, 2.5% nanocellulose, and 1% *Eucalyptus* sp. over a synthesis period of 30 hours (3 mL).

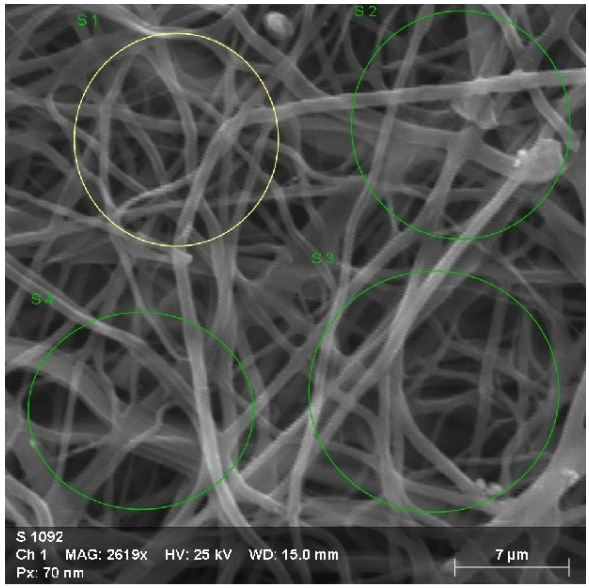

Figure 4. SEM Results and Fiber Size Distribution Histogram from PVA/NC/Alginate/ *Eucalyptus* sp.

Figure 4 indicates that the nanofibers possess an average diameter of approximately 200 nm. This structural characteristic aligns with the requirements for wound dressing applications, which typically demand nanofibers with small diameters, minimal bead formation, and homogeneity. The nanofibers were fabricated from a polymer solution consisting of 12% Poly Vinyl Alcohol (PVA), 0.5% alginate, 2.5% nanocellulose, and 1% eucalyptus extract (Euc), and were electrospun over a period of 30 hours (3 mL). The resulting nanofibers demonstrated an average diameter of 200 nm, indicating the suitability of the formulation for biomedical applications.

In this study, ImageJ was utilized to calculate the particle size distribution, with 20 replicates employed to ensure statistical reliability and minimize measurement errors. The images were initially calibrated using ImageJ, followed by the measurement of each fiber to ascertain the diameter (μm) of each particle. The resulting data was then compiled to generate a histogram that represented the particle size distribution.

The particle size distribution of the PVA/NC/Alginate/*Eucalyptus* sp. composite film, evaluated through ImageJ software, reveals significant morphological heterogeneity (Table 2). The particles exhibit mean diameters ranging from 37.00 to 116.49

Table 2. Particle Distribution Size Using the Imagej Calculation from PVA/NC/Alginate/*Eucalyptus* sp.

Frequency	Area	Mean	Min	Max	Angle	Length
1	0.058	116.485	79.000	163.062	-79.380	0.950
2	0.041	100.677	71.000	111.711	-21.801	0.628
3	0.034	78.417	63.000	94.000	-26.565	0.522
4	0.034	72.026	55.000	81.333	-49.399	0.538
5	0.031	68.611	52.000	77.375	7.125	0.470
6	0.034	76.056	68.741	87.309	32.005	0.550
7	0.024	63.500	58.000	65.444	51.340	0.374
8	0.027	65.286	52.000	71.551	33.690	0.421
9	0.031	94.141	85.500	110.000	-23.199	0.444
10	0.037	78.407	70.000	82.480	36.870	0.583
11	0.024	74.825	66.000	82.000	-45.000	0.330
12	0.027	64.735	46.000	72.000	45.000	0.412
13	0.037	56.900	37.000	68.167	-5.711	0.586
14	0.031	56.556	48.000	59.000	0.000	0.467
15	0.034	84.648	78.000	87.444	40.601	0.538
16	0.031	93.597	87.000	101.000	7.125	0.470
17	0.037	89.827	45.000	112.500	5.711	0.586
18	0.048	75.227	55.000	84.923	28.610	0.731
19	0,037	63.675	51.000	68.000	23.962	0.574
20	0,027	68.625	63.000	73.286	8.130	0.412

μm, with size extremes extending from 37.00 to 163.06 μm. Particle surface areas vary non-uniformly, indicating irregular dispersion within the matrix, potentially due to inconsistencies in mixing or drying steps. Orientation data derived from angular measurements (-79.38° to +51.34°) suggest random spatial alignment, while particle length spans from 0.33 to 0.95 units (dependent on image calibration), highlighting shape diversity. The frequency analysis shows no dominant particle class, supporting the conclusion of non-homogeneous particle distribution. Such structural irregularity can directly impact key functional attributes of the film, including its mechanical integrity, permeability, and diffusion capacity. This morphological heterogeneity should be considered in tailoring the film for biomedical or packaging applications, such as wound healing membranes or active-release bio-coatings.

The following histogram shows the data obtained from ImageJ calculations. The nanofiber size calculations were performed. The surface morphology of the nanofiber samples was characterized using Scanning Electron Microscopy coupled with Energy Dispersive X-ray Spectroscopy (SEM-EDX), and the fiber diameters were quantitatively analyzed using ImageJ software.

As depicted in Figure 5, the SEM images reveal that the synthesized nanofibers exhibit a smooth and uniform surface morphology, with no observable bead formation. SEM results particle distribution size using the ImageJ calculation histogram average diameter of 200 nm for the created nanofibers.

The Figure below is the EDS spectra data of nanofiber. This data is for the addition of 1% eucalyptus.

Figure 6 demonstrate negligible encapsulation of eucalyptus within nanofibers, as indicated by a reduction in the number of carbon atoms. The encapsulation procedure suggests that the quantity of *Eucalyptus* sp. included is inadequate, at merely 1%. Furthermore, due to the volatile nature of euca-

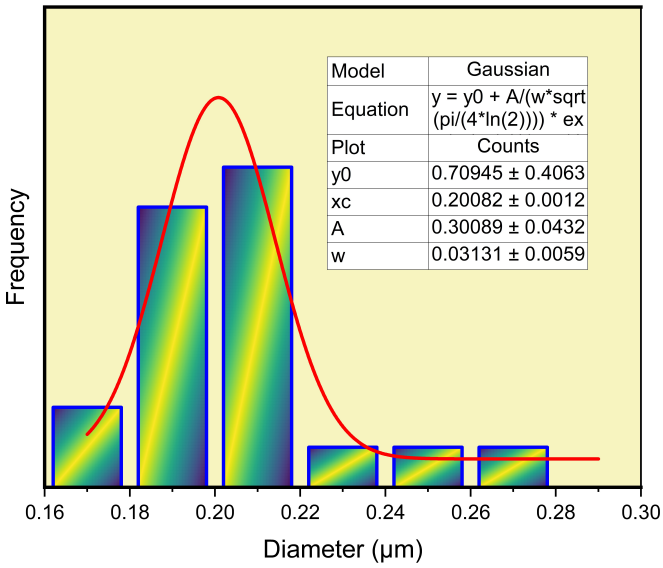

Figure 5. SEM Results Particle Distribution Size Using the Imagej Calculation Histogram Average Diameter of 200 nm for the Created Nanofibers from PVA/NC/Alginate/*Eucalyptus* sp.

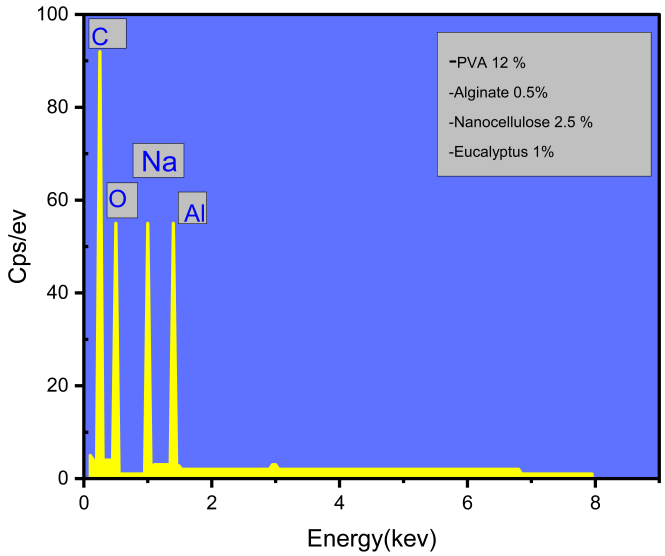

Figure 6. EDS Nanofiber from PVA/NC/Alginate/ *Eucalyptus* sp. with Addition of Eucalyptus 1%

lyptus oil, evaporation is possible during its injection into the collector. Therefore, it is imperative to augment the eucalyptus concentration in subsequent trials. The surface morphology of the nanofiber samples was examined using Bruker's SEM-EDS analysis, and the material diameter of PVA nanofiber and PVA/NC/Alginate nanofiber composites was determined using ImageJ software. The preceding text is incomplete. Figure 6 displays the outcomes of the SEM investigation of the nanofibers. The generated nanofibers have a homogeneous surface devoid of any beads. Figure 7 demonstrates that the nanofibers possess an average diameter of 0.20082 ± 0.0012 μm.

Table 3 presents the EDS (Energy Dispersive X-ray Spectroscopy) spectral data of nanofibers composed of PVA/NC/Alginate/*Eucalyptus* sp. with an additional 1% eucalyptus extract. The analysis reveals that carbon (C) and oxygen (O) are the predominant elements, with mass percentages of 81.68% and 18.10%, respectively. These values are consistent with the organic nature of the base materials-polyvinyl alcohol (PVA), nanocellulose (NC), and alginate-all of which are rich in carbon and oxygen functional groups. The atomic percentage of carbon (85.64%) is notably higher than that of oxygen (14.25%), indicating a carbon-dominant molecular structure typical of polysaccharides and natural polymers.

In addition, trace amounts of sodium (Na) and aluminum (Al) were detected, with normalized mass percentages of 0.14% and 0.07%, respectively. Sodium likely originates from sodium alginate, while aluminum may stem from contamination during sample preparation or instrument artifacts. Given their very low concentrations, these elements exhibit relatively high measurement errors (up to 42.59% relative error), and should be interpreted with caution in quantitative analysis. Overall, the EDS findings confirm that the synthesized nanofiber primarily consists of carbon and oxygen, aligning with the expected composition of natural polymer-based materials and eucalyptus-derived compounds.

3.5.2 Nanofibril Cellulose from PVA/NC/Alginate without *Eucalyptus* sp

This study investigates the presence of nanofibril cellulose in a composite material composed of polyvinyl alcohol (PVA), nanocellulose (NC), and alginate without *Eucalyptus* sp. The analysis method employed was the most current at the time of publication. The results demonstrate that nanofibers were effectively synthesized utilizing a formulation of 12% PVA, 0.5% alginate, 2.5% nanocellulose

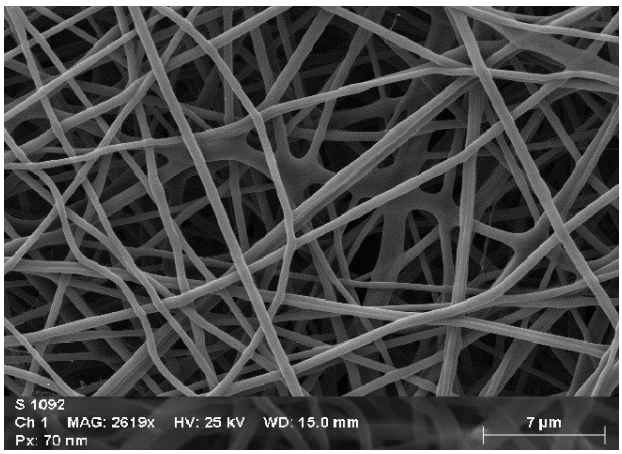

Figure 7. SEM Results and Fiber Size Distribution Histogram from PVA/NC/Alginate

The material under investigation consists of nanofibril cellulose extracted from a blend of polyvinyl alcohol, nanocellulose, and alginate, absenting any incorporation of *Eucalyptus* sp. The following are the results. They are from the particle distribution size calculation. This calculation was done using ImageJ. It used PVA/NC/Alginate. I used ImageJ to calculate the particle size distribution using 20 replicates in this SEM data study, ensuring statistical reliability and minimizing measurement errors. The images were first calibrated using ImageJ, then measurements of each fiber were made to determine the diameter of each particle, and the resulting data was compiled to produce a histogram representing the particle size distribution.

Table 4 presents the particle size distribution data of the PVA (polyvinyl alcohol)/nanocellulose (NC)/alginate composite film, as analyzed through microscopic image processing using the ImageJ software. The table includes 20 particle samples with parameters such as frequency, area, mean diameter, minimum and maximum size, orientation angle, and particle length. The average particle size (Mean) exhibits notable variation, ranging from 60.64 μm to 129.72 μm, indicating a relatively broad size distribution across the sample. The recorded minimum and maximum sizes for individual particles

Table 3. EDS Spectra Data of Nanofiber from PVA/NC/Alginate/*Eucalyptus* sp. with Addition of Eucalyptus

Element	At.No	Netto	Mass(%)	Mass Norm.(%)	Atom(%)	abs.error(%) (1 sigma)	rel.error(%) (1 sigma)
Carbon	6	122378	81.68	81.68	85.64	9.13	11.17
Oxygen	8	8108	18.10	18.10	14.25	2.64	14.58
Sodium	11	510	0.14	0.14	0.08	0.04	27.15
Aluminium	13	561	0.07	0.07	0.03	0.03	42.59
Sum			100.00	100.00	100.00		

Table 4. Particle Distribution Size Using the Imagej Calculation from PVA/NC/Alginate

Frequency	Area	Mean	Min	Max	Angle	Length
1	0.031	129.715	95.000	152.781	-39.806	0.456
2	0.051	85.728	73.000	97.000	-50.711	0.829
3	0.041	84.220	75.000	88.636	-5.194	0.644
4	0.051	109.995	45.000	141.000	-56.310	0.841
5	0.058	70.621	51.000	88.000	-86.424	0.935
6	0.041	90.986	84.000	95.959	-68.199	0.628
7	0.031	92.111	81.000	97.000	-90.000	0.467
8	0.065	76.737	64.000	88.500	-9.462	1.064
9	0.024	88.048	84.000	91.667	0.000	0.350
10	0.037	60.636	26.000	76.200	5.711	0.586
11	0.051	86.848	58.000	104.286	-81.870	0.825
12	0.048	64.923	34.000	76.308	-4.399	0.760
13	0.048	99.143	93.000	106.000	-90.000	0.758
14	0.051	76.067	69.000	80.571	-8.130	0.825
15	0.044	86.135	77.000	103.000	14.036	0.721
16	0.048	90.352	66.000	113.231	4.399	0.760
17	0.051	69.556	37.000	79.990	17.103	0.793
18	0.061	89.485	49.820	114.706	-28.072	0.992
19	0.034	65.489	58.000	69.000	-6.340	0.528
20	0.037	81.000	70.000	101.000	0.000	0.583

span from 26.00 μm to 152.78 μm, suggesting heterogeneity in particle formation. This variability is likely influenced by factors such as dispersion uniformity, the viscosity of the composite mixture, and the film casting conditions. The orientation angles of the particles range from -90° to +17.10°, reflecting a random spatial distribution of particles within the polymer matrix. The particle lengths range between 0.35 and 1.06 units (depending on the image scale, possibly in μm or mm), indicating that many of the particles exhibit elongated or irregular morphologies rather than spherical shapes. Overall, the analysis reveals that the PVA/NC/Alginate composite film contains particles with a diverse range of sizes and random orientations. These microstructural characteristics could significantly affect the film's macroscopic properties, including its mechanical strength, barrier performance, and functional behavior in various applications.

The following histogram presents the data obtained using ImageJ software. The nanofiber dimensions were measured, and the surface morphology of the nanofiber samples was analyzed using Scanning Electron Microscopy (SEM) combined with Energy Dispersive X-ray Spectroscopy (EDX). The fiber diameters were quantitatively measured with the aid of ImageJ software. The analysis revealed a relatively uniform distribution of fiber diameters, indicating consistent fabrication parameters during the electrospinning process. The SEM images provided visual confirmation of the nanofiber morphology, while EDX spectra supported the elemental composition of the samples, confirming the presence of key constituents such as carbon and oxygen. These results validate the successful synthesis of nanofibers and demonstrate the reliability of ImageJ as a tool for nanoscale measurement.

As shown in Figure 8, the scanning electron microscope (SEM) images reveal that the synthesized nanofibers have a smooth, uniform surface with no observable bead formation. The SEM results show that the average diameter of the created nanofibers is 240 nm, as calculated using the ImageJ histogram. This consistent fiber morphology suggests that the electrospinning process is stable and that the optimization of parameters has been effective. Additionally, the narrow distribution of fiber diameters indicates high reproducibility and control over the

Table 5. EDS Spectra Data of Nanofiber without *Eucalyptus* sp.

Element	At.No	Netto	Mass (%)	Mass Norm. (%)	Atom (%)	abs.error (%) (1 sigma)
Carbon	6	55315	76.01	76.33	81.34	8.92
Oxygen	8	5784	22.63	22.73	18.18	3.48
Sodium	11	2238	0.63	0.63	0.30	0.06
Aluminium	13	553	0.32	0.32	0.18	0.05
Sum			99.58	100.00	100.00	

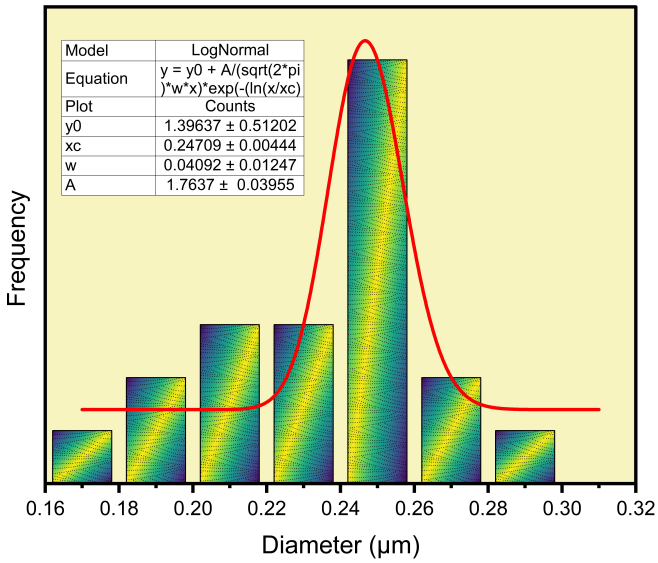

Figure 8. SEM Results Particle Distribution Size Using the Imagej Calculation Histogram Average Diameter of 240 nm for the Created Nanofibers from PVA/ Nanocellulose/Alginate

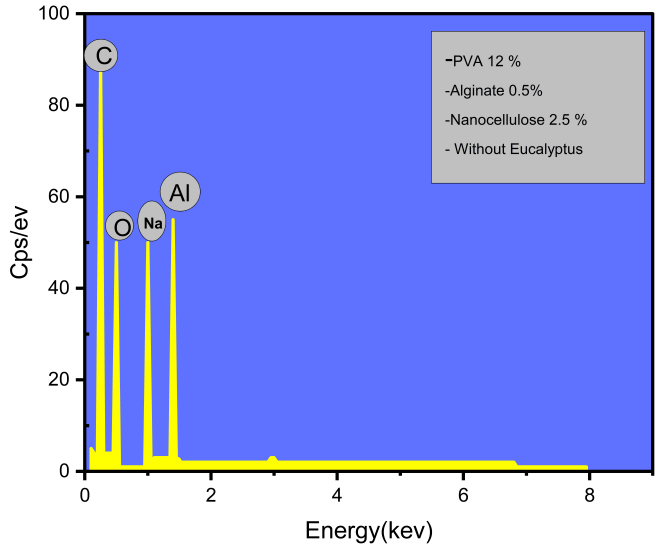

Figure 9. EDS Nanofiber without *Eucalyptus* sp.

fabrication process, which is imperative for applications necessitating uniformity in nanofiber structure, such as in biomedical scaffolds, filtration membranes, or controlled drug delivery systems.

Figure 9 show that there is negligible encapsulation of eucalyptus within the nanofibers. This is indicated by a reduction in the number of carbon atoms. The encapsulation procedure suggests that the quantity of *Eucalyptus* sp. included is inadequate at only 1%. Additionally, due to the volatile nature of eucalyptus oil, evaporation may occur during injection into the collector. Therefore, it is imperative to increase the eucalyptus concentration in subsequent trials. Bruker's SEM-EDS analysis was used to examine the surface morphology of the nanofiber samples, and ImageJ software was used to determine the material diameter of PVA nanofiber and PVA/NC/alginate nanofiber composites. The preceding text is incomplete. Figure 8 shows the results of the SEM analysis of the nanofibers possess an average diameter of $0.24709 \pm 0.00444\,\mu$m.

The elemental composition of the nanofiber sample without the addition of *Eucalyptus* sp. extract was characterized using Energy Dispersive X-ray Spectroscopy (EDS), as presented in Table 5. The analysis revealed that carbon (C) was the predominant element, accounting for 76.01% of the total mass and 81.34% of the atomic concentration. This high carbon content is consistent with the primary constituents of the nanofiber, such as polyvinyl alcohol (PVA), nanocellulose, and sodium alginate, which are rich in carbon-based functional groups. Oxygen (O) was the second most abundant element, contributing 22.63% by mass and 18.18% in atomic percentage, reflecting the presence of hydroxyl and other oxygen-containing groups typical of polysaccharides and polyols. Minor elements including sodium (Na) and aluminum (Al) were detected in trace amounts, with mass percentages of 0.63% and 0.32%, respectively. The presence of sodium likely originated from residual sodium alginate, while aluminum may be attributed to contamination from the synthesis environment or instrumentation. The total measured elemental mass was 99.58%, indicating a high accuracy of the EDS quantification. The associated absolute and relative errors (1 sigma) remained within acceptable ranges, except for aluminum which exhibited relatively high error due to its low signal intensity.

4. CONCLUSIONS

The experimental findings demonstrated that the optimum nanocellulose particle size was obtained using a 50% sulfuric acid solution at 40°C for 10 minutes, resulting in an average diameter of approximately 484.3 nm. At a higher sulfuric acid concentration of 75%, the cellulose tends to revert to its macromolecular configuration, indicating limited hydrolysis efficiency under such conditions. Fourier Transform Infrared Spectroscopy (FTIR) analysis confirmed that elevated acid concentrations do not significantly disrupt the cellulose structure, even under high-temperature hydrolysis. Furthermore, the results confirmed that polyvinyl alcohol (PVA) exhibits excellent compatibility with nanocellulose, suggesting its suitability for composite formulation and nanofiber fabrication.

The optimal concentration of polyvinyl alcohol (PVA) for nanofiber fabrication was determined to be 12%, providing favorable spinnability and structural uniformity. The strong compatibility between PVA and nanocellulose was confirmed by scanning electron microscopy (SEM), which revealed an average fiber diameter of 0.20082 ± 0.00124 μm. In contrast, nanofibers fabricated without the incorporation of *Eucalyptus* sp. exhibited a slightly larger average diameter of 0.24709 ± 0.00444 μm. This indicates that the inclusion of *Eucalyptus* sp. contributes to the refinement of fiber morphology. Furthermore, the encapsulation method applied for *Eucalyptus* sp. was found to effectively preserve the nanofiber architecture, offering a more robust and stable structure compared to conventional immobilization techniques. The encapsulation approach not only maintains the physicochemical integrity of the fibers but also potentially enhances their biofunctionality, including antimicrobial activity. Taken together, these findings highlight the promising potential of PVA/nanocellulose/*Eucalyptus* sp. based nanofiber composites for biomedical applications, particularly in advanced wound dressings and controlled drug delivery systems.

5. ACKNOWLEDGMENT

Our research was supported by Bioprocess Laboratory, Faculty of Engineering, University of Indonesia, I am grateful to Dini Kista Rianti as the laboratory staff and Prof. Dr.-Ing. Ir. Misri Gozan, M.Tech., IPU, who guided me in my research and supervised the writing. I am also grateful to the Physics Laboratory of Materials Science at Sriwijaya University, especially to Mrs. Dr. Idha Rohayani, S.Si., M.Si who guided the briefing and writing. I don't forget to thank Muhamad Ihsan for the laboratory staff who helped me in the synthesis and research.

REFERENCES

Aisy, L. A. R., T. Kemala, L. Suryanegara, and H. Purwaningsih (2024). Isolation and Characterization of Cellulose Nanofibrils (CNF) from Dates By-Product via Citric Acid Hydrolysis. *Science and Technology Indonesia*, **9**(4); 818–827

Aminsobhani, M., H. Razmi, F. Hamidzadeh, and A. Rezaei Avval (2022). Evaluation of the Antibacterial Effect of Xylene, Chloroform, Eucalyptol, and Orange Oil on Enterococcus Faecalis in Nonsurgical Root Canal Retreatment: An Ex Vivo Study. *BioMed Research International*, **2022**(1); 8176172

Apiratikul, N., P. Bunrit, S. Jommaroeng, P. Boonsri, and K. Songsrirote (2025). Synthesis and Application of Schiff Base as a Dual-Mode Chemosensor for Optical Determination of Aluminium Ion Content in Water Samples. *Sensors International*, **6**; 100313

Bacha, E. G. (2022). Response Surface Methodology Modeling, Experimental Validation, and Optimization of Acid Hydrolysis Process Parameters for Nanocellulose Extraction. *South African Journal of Chemical Engineering*, **40**(1); 176–185

Blasi, A., A. Verardi, C. G. Lopresto, S. Siciliano, and P. Sangiorgio (2023). Lignocellulosic Agricultural Waste Valorization to Obtain Valuable Products: An Overview. *Recycling*, **8**(4); 61

Chen, D., K. Cen, X. Zhuang, Z. Gan, J. Zhou, Y. Zhang, and H. Zhang (2022). Insight into Biomass Pyrolysis Mechanism Based on Cellulose, Hemicellulose, and Lignin: Evolution of Volatiles and Kinetics, Elucidation of Reaction Pathways, and Characterization of Gas, Biochar and Bio-Oil. *Combustion and Flame*, **242**; 112142

Delgado-Paredes, G. E., P. R. Delgado-Rojas, and C. Rojas-Idrogo (2021). Peruvian Medicinal Plants and Cosmopolitan Plants with Potential Use in the Treatment of Respiratory Diseases and COVID-19. *International Journal of Plant, Animal and Environmental Sciences*, **11**(2); 295–321

Deligianni, E., E. Pizzi, I. Kavelaki, I. Siden-Kiamos, F. U. Sapienza, R. Fioravanti, and R. Ragno (2023). Screening of the Activity of Sixty Essential Oils Against Plasmodium Early Mosquito Stages in Vitro and Machine Learning Analysis Reveals New Putative Inhibitors of Malaria Parasites. *International Journal for Parasitology: Drugs and Drug Resistance*, **23**; 87–93

Dheyab, A. S., A. J. K. Ibrahim, E. K. Aljumily, M. K. AlOmar, M. F. A. Bakar, and S. F. Sabran (2022). Antimycobacterial Activity and Phytochemical Properties of *Eucalyptus camaldulensis* (Eucalyptus) Extracted by Deep Eutectic Solvents. *Materials Today: Proceedings*, **65**; 2738–2742

Elbhnsawi, N. A., B. H. Elwakil, A. H. Hassanin, N. Shehata, S. S. Elshewemi, M. Hagar, and Z. A. Olama (2023). Nano-Chitosan/Eucalyptus Oil/Cellulose Acetate Nanofibers: Manufacturing, Antibacterial and Wound Healing Activities. *Membranes*, **13**(6); 604

Fan, M., C. Li, Y. Sun, L. Zhang, S. Zhang, and X. Hu (2021). In Situ Characterization of Functional Groups of Biochar in Pyrolysis of Cellulose. *Science of the Total Environment*, **799**; 149354

Flerlage, T., D. F. Boyd, V. Meliopoulos, P. G. Thomas, and S. Schultz-Cherry (2021). Influenza Virus and SARS-CoV-2: Pathogenesis and Host Responses in the Respiratory Tract. *Nature Reviews Microbiology*, **19**(7); 425–441

Fletes-Vargas, G., H. Espinosa-Andrews, J. M. Cervantes-Uc, I. Limón-Rocha, G. Luna-Bárcenas, M. Vázquez-Lepe, and P. Ramos-Martínez (2023). Porous Chitosan Hydrogels Produced by Physical Crosslinking: Physicochemical, Structural, and Cytotoxic Properties. *Polymers*, **15**(9); 2203

Galan, D. M., N. E. Ezeudu, J. Garcia, C. A. Geronimo, N. M. Berry, and B. J. Malcolm (2020). Eucalyptol (1,8-Cineole): An Underutilized Ally in Respiratory Disorders. *Journal of Essential Oil Research*, **32**(2); 103–110

Goscianska, J., R. Freund, and S. Wuttke (2022). Nanoscience Versus Viruses: The SARS-CoV-2 Case. *Advanced Functional Materials*, **32**(14); 2107826

Gupta, A., P. Ayithapu, and R. Singhal (2021). Study of the Electric Field Distribution of Various Electrospinning Geometries and Its Effect on the Resultant Nanofibers Using Finite Element Simulation. *Chemical Engineering Science*, **235**; 116463

Jafari, F., M. Ramezani, H. Nomani, M. S. Amiri, A. T. Moghadam, A. Sahebkar, and A. H. Mohammadpour (2021). Therapeutic Effect, Chemical Composition, Ethnobotanical Profile of *Eucalyptus globulus*: A Review. *Letters in Organic Chemistry*, **18**(6); 419–452

Kazemzadeh, G., N. Jirofti, H. Kazemi Mehrjerdi, M. Rajabioun, S. A. Alamdaran, D. Mohebbi-Kalhori, and R. Taheri (2022). A Review on Developments of In-Vitro and In-Vivo Evaluation of Hybrid PCL-Based Natural Polymers Nanofibers Scaffolds for Vascular Tissue Engineering. *Journal of Industrial Textiles*, **52**; 15280837221128314

Kim, D., M.-K. Kang, and Y.-H. Kang (2020). Eucalyptol Blocks Diabetes-Associated Disruption of Tight Junction and Blood Retinal Barrier in Retinal Pigment Epithelial Cells and Diabetic Eyes. *Current Developments in Nutrition*, **4**; 045–046

Kumar, R., S. Sivaganesan, P. Senthamaraikannan, S. Saravanakumar, A. Khan, S. Ajith Arul Daniel, and L. Loganathan (2022). Characterization of New Cellulosic Fiber from the Bark of *Acacia nilotica* L. Plant. *Journal of Natural Fibers*, **19**(1); 199–208

Liñán-Atero, R., F. Aghababaei, S. R. García, Z. Hasiri, D. Ziogkas, A. Moreno, and M. Hadidi (2024). Clove Essential Oil: Chemical Profile, Biological Activities, Encapsulation Strategies, and Food Applications. *Antioxidants*, **13**(4); 488

Low, Z. L., D. Y. S. Low, S. Y. Tang, S. Manickam, K. W. Tan, and Z. H. Ban (2022). Ultrasonic Cavitation: An Effective Cleaner and Greener Intensification Technology in the Extraction and Surface Modification of Nanocellulose. *Ultrasonics Sonochemistry*, **90**; 106176

Maftuchah, M., P. I. Christine, and M. Jamaluddin (2020). The Effectiveness of Tea Tree Oil and Eucalyptus Oil Aromatherapy for Toddlers with Common Cold. *Jurnal Kebidanan*, **10**(2); 131–137

Malakar, M. (2024). *Eucalyptus* sp. : A Wonder Tree. In *Advances in Medicinal and Aromatic Plants*. Apple Academic Press, pages Vol1: 185–Vol181: 260

Mallakpour, S., Z. Radfar, and C. M. Hussain (2021). Current Advances on Polymer-Layered Double Hydroxides/Metal Oxides Nanocomposites and Bionanocomposites: Fabrications and Applications in the Textile Industry and Nanofibers. *Applied Clay Science*, **206**; 106054

Md Salim, R., J. Asik, and M. S. Sarjadi (2021). Chemical Functional Groups of Extractives, Cellulose and Lignin Extracted from Native *Leucaena leucocephala* Bark. *Wood Science and Technology*, **55**; 295–313

Meijaard, E., T. M. Brooks, K. M. Carlson, E. M. Slade, J. Garcia-Ulloa, D. L. Gaveau, and M. J. Struebig (2020). The Environmental Impacts of Palm Oil in Context. *Nature Plants*, **6**(12); 1418–1426

Natrayan, L., A. Merneedi, G. Bharathiraja, S. Kaliappan, D. Veeman, and P. Murugan (2021). Processing and Characterization of Carbon Nanofibre Composites for Automotive Applications. *Journal of Nanomaterials*, **2021**(1); 7323885

Park, M. K., J. Y. Cha, M. C. Kang, H. W. Jang, and Y. S. Choi (2024). The Effects of Different Extraction Methods on Essential Oils from Orange and Tangor: From the Peel to the Essential Oil. *Food Science & Nutrition*, **12**(2); 804–814

Patel, J. K., A. Patel, and D. Bhatia (2021). Introduction to Nanomaterials and Nanotechnology. In *Emerging Technologies for Nanoparticle Manufacturing*. Springer, pages 3–23

Pawcenis, D., M. Leśniak, M. Szumera, M. Sitarz, and J. Profic-Paczkowska (2022). Effect of Hydrolysis Time, pH and Surfactant Type on Stability of Hydrochloric Acid Hydrolyzed Nanocellulose. *International Journal of Biological Macromolecules*, **222**; 1996–2005

Pimenta, J., C. Dias, M. Cotovio, and M. J. Saavedra (2023). In Vitro Effect of Eucalyptus Essential Oils and Antiseptics (Chlorhexidine Gluconate and Povidone-Iodine) Against Bacterial Isolates from Equine Wounds. *Veterinary Sciences*, **11**(1); 12

Pimenta, M., A. Marucci, S. Brown, M. Matthews, A. Rao, P. Eklund, and M. Dresselhaus (1998). Resonant Raman Effect in Single-Wall Carbon Nanotubes. *Journal of Materials Research*, **13**(9); 2396–2404

Rawat, A., M. Rawat, O. Prakash, R. Kumar, H. Punetha, and D. S. Rawat (2022). Comparative Study on Eucalyptol and Camphor Rich Essential Oils from Rhizomes of *Hedychium spicatum* sm. and Their Pharmacological, Antioxidant and Antifungal Activities. *Anais Da Academia Brasileira De Ciências*, **94**; e20210932

Rehman, R., W. Ahmad, R. Muzaffar, A. Bano, I. Sajid, A. U. Ahsan, and U. Naeem (2024). Insect Repellent and Insecticidal Potential of Two Eucalyptus Species Essential Oils from Subtropical Desert Climate. *Chemical Papers*, **78**(4); 2369–2384

Shoukat, R. and M. I. Khan (2021). Carbon Nanotubes: A Review on Properties, Synthesis Methods and Applications in Micro and Nanotechnology. *Microsystem Technologies*, **27**; 4183–4192

Susi, S., M. Ainuri, W. Wagiman, and M. Falah (2022). Effect of Delignification and Bleaching Stages on Cellulose Purity

of Oil Palm Empty Fruit Bunches. In *IOP Conference Series: Earth and Environmental Science*, volume 1116. page 012018

Syahza, A. and B. Asmit (2020). Development of Palm Oil Sector and Future Challenge in Riau Province, Indonesia. *Journal of Science and Technology Policy Management*, **11**(2); 149–170

Tu, H., M. Zhu, B. Duan, and L. Zhang (2021). Recent Progress in High-Strength and Robust Regenerated Cellulose Materials. *Advanced Materials*, **33**(28); 2000682

Tuhmaz, G. (2024). *Perspective Chapter: Sustainable Nanofibers and Their Applications*. IntechOpen

Veerendranadh, Y., D. Ramarao, and U. Sambamoorthy (2018). Fundamentals of Eucalyptus Oil Extraction and Use. Unpublished work or book chapter (publisher and year not specified)

Vârban, R., I. Crișan, D. Vârban, A. Ona, L. Olar, A. Stoie, and R. Ștefan (2021). Comparative FT-IR Prospecting for Cellulose in Stems of Some Fiber Plants: Flax, Velvet Leaf, Hemp and Jute. *Applied Sciences*, **11**(18); 8570

Wang, L., K. Li, K. Copenhaver, S. Mackay, M. E. Lamm, X. Zhao, and D. Neivandt (2021). Review on Nonconventional Fibrillation Methods of Producing Cellulose Nanofibrils and Their Applications. *Biomacromolecules*, **22**(10); 4037–4059

Wohlert, M., T. Benselfelt, L. Wågberg, I. Furó, L. A. Berglund, and J. Wohlert (2022). Cellulose and the Role of Hydrogen Bonds: Not in Charge of Everything. *Cellulose*; 1–23

Zhang, Q., E. Zhu, T. Li, L. Zhang, and Z. Wang (2024). High-Value Utilization of Cellulose: Intriguing and Important Effects of Hydrogen Bonding Interactions- A Mini-Review. *Biomacromolecules*, **25**(10); 6296–6318

Zhou, M., D. Chen, Q. Chen, P. Chen, G. Song, and C. Chang (2024). Reversible Surface Engineering of Cellulose Elementary Fibrils: From Ultralong Nanocelluloses to Advanced Cellulosic Materials. *Advanced Materials*, **36**(21); 2312220

